β3-adrenergic blockade targets fatty acid oxidation to induce ferroptotic vulnerability in pediatric T-ALL

Cristina Banella
cristina.banella@meyer.it
Meyer Children's Hospital IRCCS
Serena Travaglini
University of Rome Tor Vergata
Francesco Carrozzo
Meyer Children's Hospital IRCCS
Agnese Roveta
Meyer Children's Hospital IRCCS
Francesco Pegoraro
Meyer Children's Hospital IRCCS
Gianluca Mattei
Meyer Children's Hospital
Rachele Amato
Meyer Children's Hospital
Maria Ascone
Meyer Children's Hospital IRCCS
Federica De Luca
Meyer Children's Hospital IRCCS
Aurora Chinnici
Meyer Children's Hospital IRCCS
Cinzia Marchi
Meyer Children's Hospital
Elena Chiocca
Meyer Children's Hospital IRCCS
Annalisa Tondo
Meyer Children's Hospital IRCCS
Marinella Veltroni
Meyer Children's Hospital IRCCS
Maura Calvani

Meyer Children’s Hospital IRCCS

Research Article

Keywords: Acute Lymphoblastic Leukemia, metabolism, ferroptosis, fatty acid oxidation, adrenergic receptor

Posted Date: April 22nd, 2026

DOI: https://doi.org/10.21203/rs.3.rs-9392453/v1

Additional Declarations: No competing interests reported.

β3-adrenergic blockade targets fatty acid oxidation to induce ferroptotic vulnerability in pediatric T-ALL

Cristina Banella[1*], Serena Travaglini[2*], Francesco Carrozzo[1], Agnese Roveta[1,3], Francesco Pegoraro[1,4], Gianluca Mattei[5], Rachele Amato[6], Maria Ascone[1], Federica De Luca[1], Aurora Chinnici[1], Cinzia Marchi[7], Elena Chiocca[1], Annalisa Tondo[1], Marinella Veltroni[1#], Maura Calvani[1#]

[1]Department of Pediatric Hematology-Oncology, Meyer Children's Hospital IRCCS, Florence, Italy.
[2]Department of Experimental Medicine, University of Rome Tor Vergata, Rome, Italy.
[3]Department of Health Science, University of Florence, Florence, Italy
[4]Department of Experimental and Clinical Medicine, University of Florence, Florence, Italy
[5]Department of Neuroscience and Human Genetics, Meyer Children's Hospital IRCCS, Florence, Italy.
[6]Department of Pediatric Neuro-Oncology, Meyer Children's Hospital IRCCS, Florence, Italy.
[7]Clinical Chemistry and Microbiology Laboratory, Meyer Children's Hospital IRCCS, Florence, Italy.

*# Equal contributors

Correspondence:
Cristina Banella, PhD
Department of Pediatric Hematology-Oncology, Meyer Children's Hospital IRCCS, 50139 Florence, Italy; e-mail: cristina.banella@meyer.it

Running Title: SR59230A Induces FAO-Dependent Ferroptosis

Data availability

Data will be made available on request to the corresponding author.

The raw DNA methylation data (.idat files) as well as the matrix with the raw counts, generated for this study, have been deposited in the NCBI Gene Expression Omnibus (GEO) and are accessible through accession number GSE324557.

text word count: 3596

abstract word count: 242

number of figures: 6

number of tables: 0

number of references: 65

Abstract

Pediatric T-cell acute lymphoblastic leukemia (T-ALL) accounts for approximately 15% of childhood ALL and is associated with a high risk of relapse, with ~25% of patients failing conventional therapy. Resistance is driven by pro-survival signaling, impaired apoptosis, and metabolic adaptations that sustain leukemic proliferation under stress. Herein, we investigate the role of β3-adrenergic receptor (β3-AR) antagonist SR59230A signaling in the metabolic reprogramming and therapeutic vulnerability of pediatric T-ALL.

β3-AR expression and transcriptomic profiling following SR59230A exposure were assessed in T-ALL cell lines by RNA sequencing, followed by gene set enrichment analysis of Gene Ontology and Hallmark pathways. Metabolic alterations were validated by Seahorse analyses of mitochondrial respiration, glycolysis, fatty acid oxidation (FAO), and fuel dependency. Systemic iron metabolism was evaluated by ferritin and free iron quantification using COBAS8000.

β3-AR was markedly upregulated in T-ALL cells compared with normal hematopoietic counterparts, identifying a selective metabolic vulnerability. Pharmacologic inhibition of β3-AR with SR59230A affected mitochondrial oxidative phosphorylation, with a predominant effect on complex I activity, and suppressed FAO. This metabolic collapse disrupted bioenergetic flexibility and triggered ferroptotic cell death, accompanied by modulation of ferritin and transferrin levels, suggesting their potential role as biomarkers of metabolic response. Importantly, β3-AR blockade sensitized T-ALL cells to oxidative phosphorylation inhibition, resulting in synergistic cytotoxicity in refractory models.

Collectively, these findings identify β3-AR as a central regulator of metabolic plasticity in pediatric T-ALL and uncover a basis to explore combined strategies targeting metabolic and iron-dependent vulnerabilities in high-risk disease.

Key Words

65 Acute Lymphoblastic Leukemia, metabolism, ferroptosis, fatty acid oxidation, adrenergic
66 receptor
67

Introduction

Acute lymphoblastic leukemia (ALL) represents the most common malignancy in childhood, with T-cell ALL (T-ALL) accounting for approximately 10-15% of cases.[1] Despite historically considered an aggressive subtype, the survival rate has improved over the years, with a 5-year event-free survival of 70-80% in recent patients treated with MRD-guided intensive therapy.[2–4] This progress reflects improved multi-agent therapies, refined risk stratification, early treatment response assessment, and advances in supportive care. Nevertheless, treatment resistance remains a major clinical challenge. Approximately 25% of pediatric T-ALL patients relapse, often with a more aggressive and treatment-resistant disease, resulting in a very poor prognosis.[5–7] Resistance arises from multiple mechanisms, including alterations of drug targets, pro-survival signaling, defective cell death induction, and metabolic adaptation of leukemic cells.[8–11] Therefore, the identification of novel therapeutic targets might enhance the efficacy of current treatments and help to tailor therapeutic intervention to overcome resistance.

In recent years, increasing evidence has highlighted cellular metabolism as a key regulator of leukemic cell survival, transformation, and disease progression. Metabolic adaptations allow leukemic cells to survive therapeutic pressure and dynamic microenvironmental conditions, supporting tumor maintenance and relapse.[12–15] Accordingly, metabolic targeting strategies have been investigated in hematologic malignancies. In acute myeloid leukemia (AML), IDH1/2 inhibitors[16–18] and venetoclax[19–21] have validated metabolic targeting as a therapeutic strategy. Venetoclax also demonstrates preclinical activity in T-ALL[22–27], highlighting the relevance of mitochondrial metabolism in this disease. Although metabolism-targeting agents such as antifolates are central to ALL therapy, the broader metabolic landscape underlying treatment response and resistance remains poorly defined.[28]

Among emerging metabolic regulators, the β3-adrenergic receptor (β3-AR) is increasingly linked to the regulation of lipid metabolism and glucose homeostasis in cancer cells. β3-AR signaling has been implicated in several aspects of malignant transformation, including cell proliferation, apoptosis, chemotaxis, angiogenesis, tumor growth, and modulation of the immune response.[29–33] Notably, a selective β3-AR antagonist (SR59230A) has shown direct anti-leukemic activity by promoting apoptosis, particularly under hypoxic conditions.[34] In this study, we aimed to characterize the functional role of β3-AR in the pathogenesis and treatment response of pediatric T-ALL. We investigated β3-AR expression in T-ALL models and primary samples, assessed the impact of β3-AR inhibition on cell viability, and characterized associated metabolic alterations using transcriptomic and functional analyses. By elucidating the contribution of β3-AR–driven metabolic plasticity, this work provides new insights into previously underexplored metabolic vulnerabilities in pediatric T-ALL. These findings may uncover how leukemic cells escape current therapeutic strategies and support the development of personalized approaches to overcome drug resistance in pediatric T-ALL.

Materials and Methods

Primary Patients Samples and Controls

The bone marrow (BM) sample was collected from a patient with newly diagnosed de novo T-ALL (Supplemental Table 1) admitted at the Meyer Children's Hospital IRCCS in Florence, following a collection of informed consent from parents under ethical committee approval (CET_14/2023). Age matched healthy donor Normal Peripheral Blood Mononuclear Cells (PBMCs), were used as controls.

Cell lines and cell culture

CCRF-CEM, Molt-3, and Jurkat human T-cell leukemia lines derived from a pediatric T-ALL exhibiting an immature T-cell phenotype were purchased from the American Type Culture Collection (ATCC) (Manassas, VA, USA). Cell details are listed in supplemental Methods Table 2.

Cells were cultured in RPMI 1640 medium (Euroclone, Pero, MI, Italy) supplemented with 10% fetal bovine serum (FBS; GIBCO-BRL), 20 mM HEPES, 100 U/mL penicillin, and 100 µg/mL streptomycin (GIBCO-BRL). Cultures were maintained at 37 °C in a humidified incubator with 5% CO_2.

Drug treatments

Cells were treated with SR59230A (10-50 µM for 24, 48 0r 72 h, or with RLS3 0,3 µM for 3 h) to induce ferroptosis. Where indicated, cells were also exposed to the iron chelator deferoxamine (DFX) 0,1 µM, alone or in combination with SR.

Cell Viability

A CellTiter 96® AQueous One Solution Cell Proliferation Assay was used to assess cell viability. T-ALL cells were seeded in 96-well plates (1.5–2 × 10^4 cells/well) and treated with SR59230A (10–50 µM) for 24, 48, or 72 h. For the MTS-based assay, 5 µL of reagent was added and absorbance measured at 490 nm using a microplate reader (Thermo Scientific™ Varioskan™ Flash Multimode Reader, Waltham, MA, USA).

Protein extraction and Western Blot analysis

Cell pellets were lysed in RIPA buffer with protease and phosphatase inhibitors. Equal amounts of protein were separated by SDS-PAGE, transferred to membranes, and probed with antibodies listed in supplemental Methods Table 3. Detection was performed with HRP-conjugated secondary antibodies and chemiluminescence. Signals were quantified with

ImageJ and normalized to total protein per lane. Full experimental details are provided in the Supplementary Methods.

Cytofluorimetric Analysis

The markings were performed using 0.5 x 106 cells resuspended in a volume of 100 µL of current buffer (PBS + 2% FBS + 0.5% EDTA 500mM). Cells were labeled with anti-β3-PE (Biorbyt Cat# orb124479, RRID:AB_2783863). The analysis of the samples was performed using MACSQuant Analyzer 10 Flow Cytometer (Miltenyi Biotec, Gladbach, Germany). Data were processed using Flowlogic software (Miltenyi Biotec, Gladbach, Germany).

Metabolic Assays

T-ALL cell lines and primary blasts were seeded in precoated XFe96 plates and treated with drugs as indicated. Mitochondrial respiration, glycolysis, ATP production, and fuel flexibility were assessed using the Seahorse XFe96 analyzer (Agilent Technologies). Detailed protocols, drug concentrations, and assay parameters are listed in Supplemental Methods.

Quantitative Real-Time Expression Analysis

Quantitative Reverse Transcription-Polymerase Chain Reaction (qRT-PCR) was used to evaluate the expression level of *GPX4*, *FPS1* and *NRF2* (Table SM 5*)*. See supplemental Methods for detail.

RNA sequencing

Transcriptome sequencing was performed by BGI Genomics (BGI, China). See supplemental Methods for detail.

Cobas 8000 Analyzer Assays

Ferritin quantification was performed using the Cobas® 8000 e602 module with electrochemiluminescence immunoassay (ECLIA) technology (Elecsys Ferritin, ref. 07027273190). Free iron was measured photometrically on the c702 module at 700/570 nm using the FerroZine method (IRON2, Iron Gen2, ref. 05169291190).

Statistical analysis

Data were analyzed using GraphPad Prism 10 (GraphPad Software INc., San Diego, CA, USA). Data were presented as the mean ± SD from at least three independent experiments, and each experiment was performed in triplicate. Statistical analyses were performed using the Student's *t*-test, Mann–Whitney test, Kruskal–Wallis one-way ANOVA and Dunn's post hoc tests or the one-way ANOVA and Tukey's multiple comparison test, as indicated. Statistical significance was established at $p < 0.05$.

Results

The β3-Adrenergic receptor is highly expressed in T-ALL and represents a selective therapeutic vulnerability

To characterize β3-AR expression in T-ALL, we performed flow cytometric analysis in CCRF-CEM, Molt-3, and Jurkat cell lines and compared receptor levels with healthy PBMCs. T-ALL cell lines displayed significantly higher β3-AR expression than normal PBMCs (**Fig 1A**), with β3-AR positivity of approximately 65% in CCRF-CEM, 40% in Molt-3, 35% in Jurkat cells, and only ~5% in control PBMCs.

We subsequently evaluated the therapeutic potential of the selective β3-AR antagonist SR59230A. Increasing concentrations of SR59230A (0–50 μM) for 24, 48, and 72 hours induced a significant reduction in cell viability in T-ALL cells, in a dose- and time-dependent fashion, while normal PBMCs were unaffected under the same conditions (**Fig 1B**),

196 indicating selective cytotoxicity toward leukemic cells. Notably, the anti-leukemic activity of
197 SR59230A was further enhanced under fetal bovine serum (FBS)-deprived conditions,
198 consistent with a role for β3-AR in fatty acid metabolism and bioenergetics (**Fig 1C**).
199 To further investigate SR59230A specificity, we measured adrenergic receptor family
200 members following treatment (15 μM) for 24, 48, and 72 hours. Despite SR59230A shows
201 higher affinity for β3-AR (IC50 ≈ 40 nM), it retains measurable activity toward β1 and β2
202 isoforms (IC50 ≈ 408 nM and ≈ 648 nM, respectively). No significant changes in *ADRB1* or
203 *ADRB2* transcripts were observed at any time point (**Fig 1D-E**). In contrast, *ADRB3* was
204 significantly upregulated in CCRF-CEM cells at 24 hours ($p<0.01$), in Jurkat cells at 24 and
205 48 hours ($p<0.001$ and $p<0.01$, respectively), and in Molt-3 cells at 48 hours ($p<0.0001$),
206 while decreasing in Molt-3 at 72h ($p<0.01$) (**Fig 1F**).
207 At the protein level, β3-AR expression was significantly modulated in all three T-ALL cell
208 lines following SR exposure, in agreement with transcriptional changes and consistent with
209 ligand-induced receptor downregulation (**Fig 1G** and **Fig S3C-E**). While changes in receptor
210 expression do not prove isoform-selective inhibition, it supports preferential engagement of
211 the β3-AR axis in T-ALL cells.

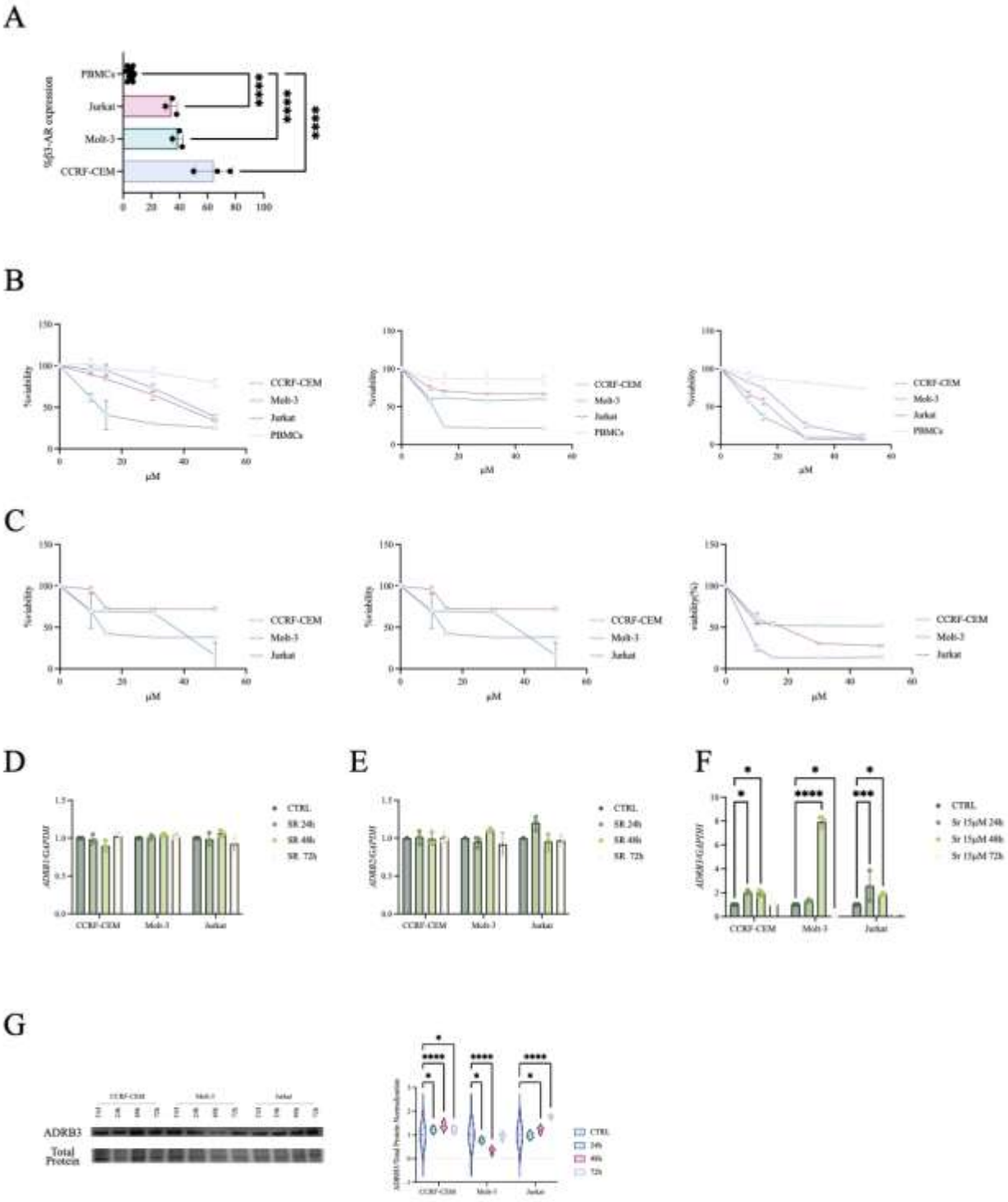

212

213

214 *SR59230A triggers convergent mitochondrial suppression and metabolic rewiring in T-ALL*

215 To investigate the transcriptional consequences of SR59230A, we performed RNAseq in T-

216 ALL models after 24h of treatment. DESeq2 analysis revealed distinct transcriptional

responses across the three cell lines (**Fig S2A**). GSEA of Hallmark pathways revealed a partially overlapping metabolic response together with lineage-specific response to SR59230A. Several pathways related to stress response, cellular signaling, and metabolic regulation were differentially modulated across the three models, reflecting context-dependent remodeling of transcriptional programs (**Fig 2A**).

Oxidative phosphorylation (OXPHOS) was the only metabolic pathway consistently downregulated in all three cell lines, with a stronger decrease in CCRF-CEM and Molt-3 cells than in Jurkat. This attenuated transcriptional response in Jurkat may reflect lower β3-AR expression and intrinsic metabolic flexibility. **Fig S2B** shows the databases GO Biological Processes, GO Cellular Components, and Hallmarks related to the mitochondria that are commonly upregulated in CCRF-CEM and Molt-3 cells, highlighting the stronger transcriptional response in these lines. Overall, these data reveal a convergent inhibition of mitochondrial respiration with lineage-specific metabolic adaptations.

To further dissect OXPHOS signature, we examined leading edge genes contributing to pathway enrichment. Shared components included multiple subunits of mitochondrial respiratory chain Complex I (*NDUFA1, NDUFA2, NDUFA3, NDUFA4, NDUFA6, NDUFB1, NDUFB2, NDUFB3, NDUFB4, NDUFB6, NDUFAB1,* and *NDUFS4*), Complex III (*UQCRB, UQCRQ, UQCR10,* and *UQCRFS1*), Complex IV (*COX5B, COX6A1, COX6C, COX7A2, COX7B, COX7C, COX8A,* and *COX17*), and ATP synthase subunits (*ATP5F1E, ATP5ME, ATP5MG, ATP5PF,* and *ATP5PO*) (**Fig 2B**), together with genes involved in mitochondrial transport, redox homeostasis (*VDAC2, SLC25A5, MPC1, TIMM8B, PRDX3,* and *GPX4*), protein import and iron–sulfur cluster biology (*HSPA9*, *FXN*, and *ISCA1)*. This profile indicates that SR59230A affects the structural and functional integrity of the entire mitochondrial respiratory machinery.

Applying refined filtering criteria (p-value<0.05 and FDR<0.1), we identified 6 Differentially Expressed Genes (DEGs) shared by all the cell lines (**Fig 2C**), including three upregulated

genes *(KLHL24, MFGE8, SLC5A3*) and three downregulated genes *(ALAS1, THOC6, RGL4)* (**Fig 2D**). Notably, *ALAS1*, a key regulator of heme biosynthesis, was part of the OXPHOS leading-edge subset, supporting mitochondrial and iron-related metabolic involvement, while genes such as *SLC5A3* suggest the activation of adaptive stress responses.

Together, these data demonstrate that SR59230A induces a convergent suppression of OXPHOS across T-ALL models, alongside context-dependent metabolic rewiring.

A

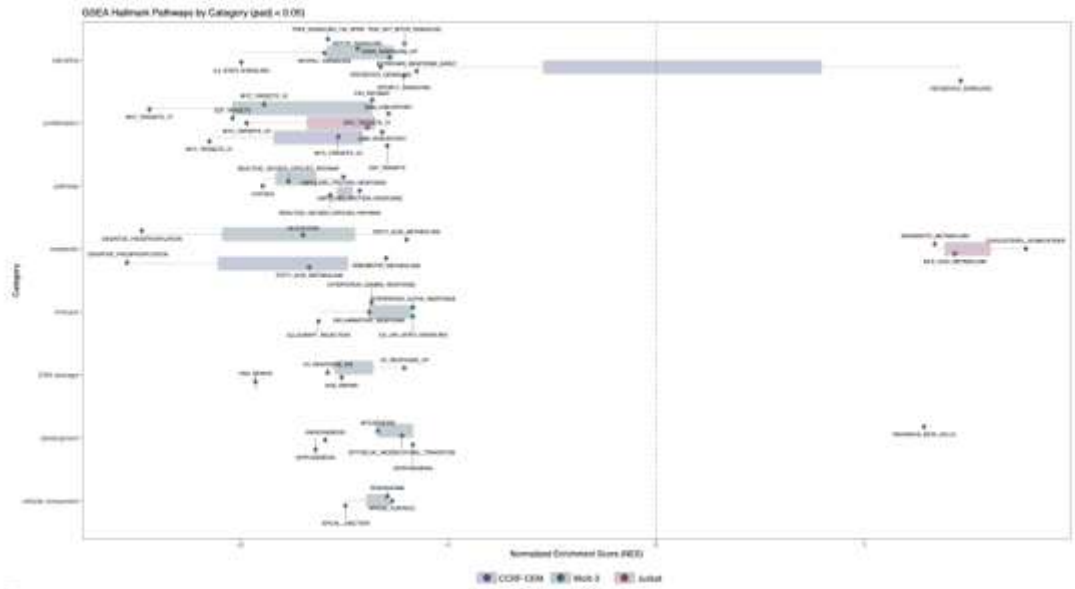
GSEA Hallmark Pathways by Category (padj < 0.05)
Category
Normalized Enrichment Score (NES)
CCRF-CEM
Molt-3
Jurkat

B

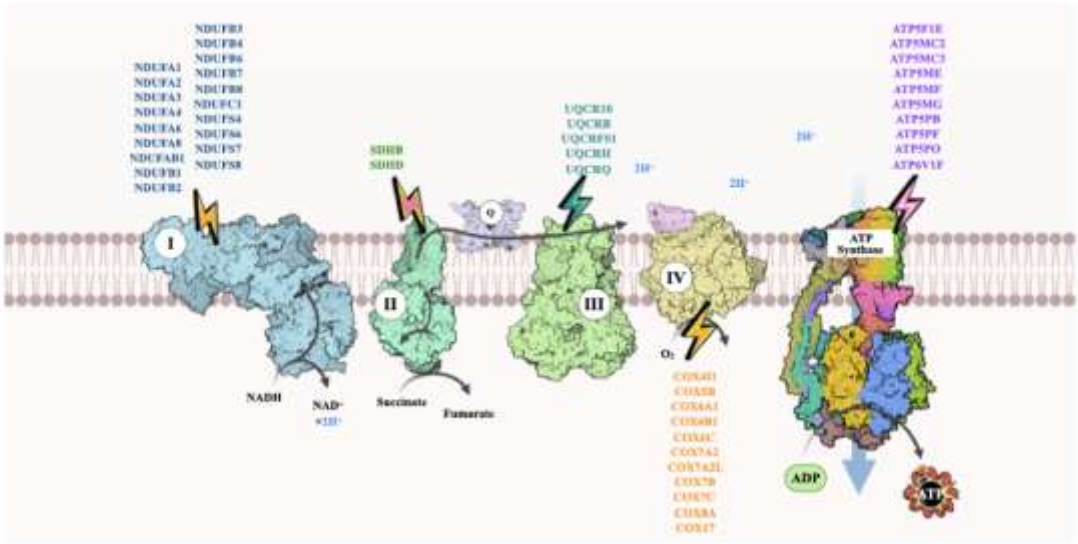
NDUFB3
NDUFB4
NDUFB6
NDUFB7
NDUFB8
NDUFC1
NDUFS4
NDUFS6
NDUFS7
NDUFS8
NDUFA1
NDUFA2
NDUFA3
NDUFA4
NDUFA6
NDUFA8
NDUFAB1
NDUFB1
NDUFB2
SDHB
SDHD
UQCR10
UQCRB
UQCRFS1
UQCRH
UQCRQ
ATP5PF1E
ATP5MC2
ATP5MC3
ATP5ME
ATP5MF
ATP5MG
ATP5PB
ATP5PF
ATP5PO
ATP6V1F
I
II
III
IV
ATP Synthase
NADH
NAD+
Succinate
Fumarate
ADP

C

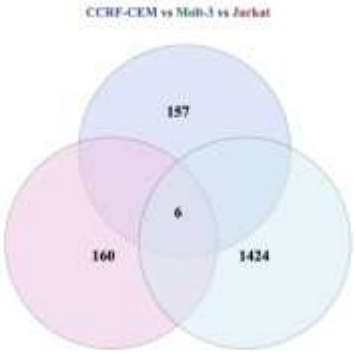
CCRF-CEM vs Molt-3 vs Jurkat
157
6
160
1424

250

SR59230A selectively impairs mitochondrial and glycolytic metabolism in T-ALL cells models

To functionally validate the metabolic impact of SR59230A, we assessed mitochondrial and glycolytic functions using Seahorse metabolic assays.

SR59230A significantly reduced basal respiration (**Fig 3A**), maximal respiration (**Fig 3B**), and spare respiratory capacity (**Fig 3C**), leading to a marked decrease in ATP production rate (**Fig 3D**) in all three leukemic models, indicating broad impairment of mitochondrial bioenergetic capacity upon SR59230A administration.

We subsequently evaluated the impact of SR59230A on glycolytic metabolism. SR59230A significantly reduced basal glycolysis in CCRF-CEM and Molt-3 cells ($p<0.001$ and $p<0.0001$, respectively), whereas Jurkat cells displayed increased basal glycolysis ($p<0.01$) (**Fig 3E**). Similarly, compensatory glycolysis was reduced in CCRF-CEM and Molt-3 cells, while no significant changes were detected in Jurkat cells (**Fig 3F**). These findings indicate that SR59230A selectively disrupts metabolic homeostasis in leukemic cells, without affecting normal PBMCs, and identify Jurkat cells as the least sensitive model, likely because compensatory glycolysis partially offsets mitochondrial ATP loss.

The same analyses were performed in PMBCs from ten healthy donors. Following 24 hours of 15 µM SR59230A, a modest reduction in basal respiration was observed ($p<0.01$) (**Fig S2A**) with no changes in maximal respiration (**Fig S2B**), spare respiratory capacity (**Fig S2C**), or total ATP production (**Fig S2D**). SR59230A also resulted in a significant reduction in proton leak ($p<0.01$) (**Fig S1E**), suggestive of improved mitochondrial efficiency and reduced uncoupled proton efflux (**Fig S2F**). No significant alterations were observed in glycolytic parameters (**Fig S2G–I**) or in mitochondrial and glycolytic ATP production rates (**Fig S2J-L**).

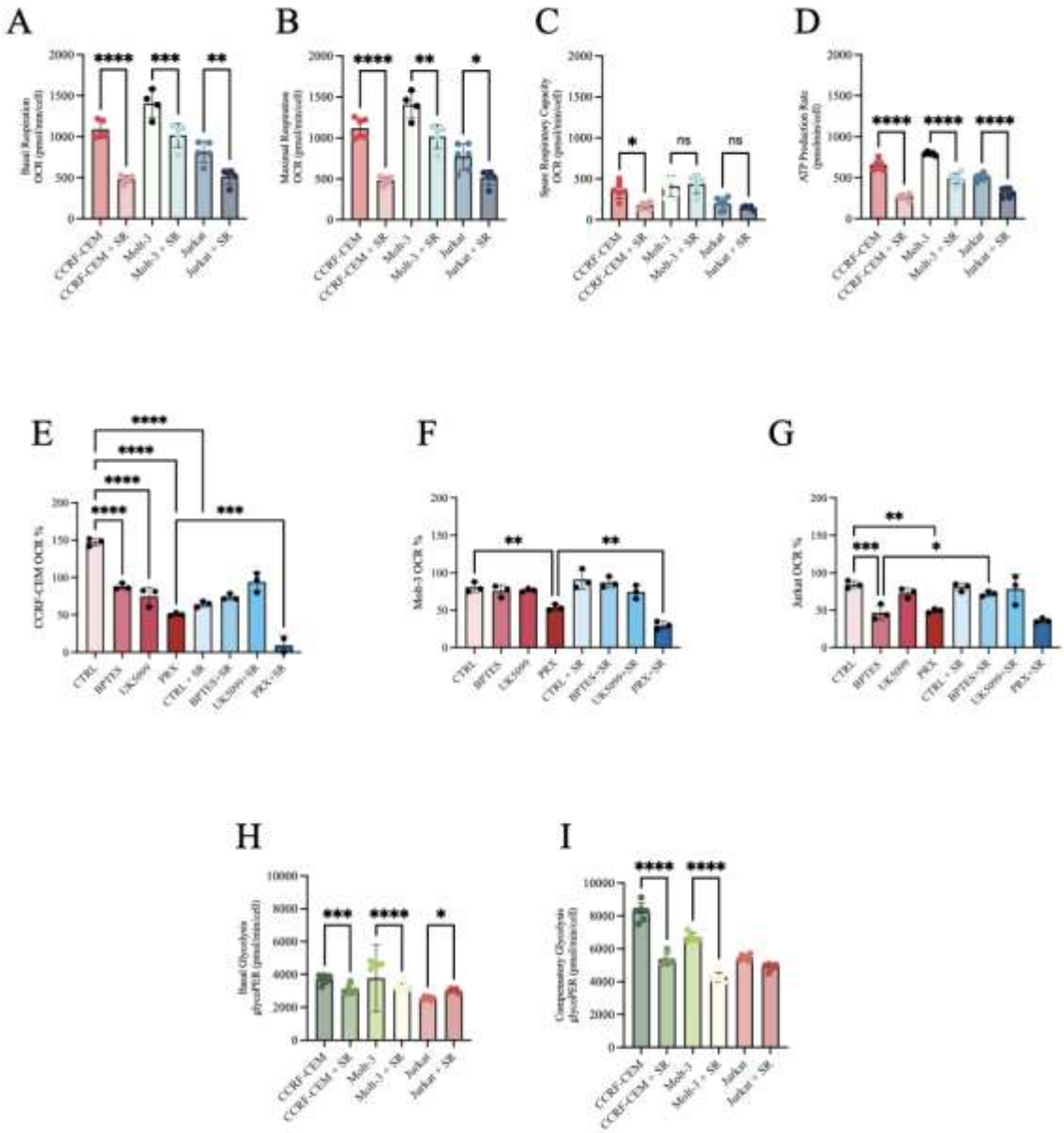

SR59230A disrupts mitochondrial bioenergetics in primary T-ALL blasts

To assess the translational relevance of our findings, we next investigated the effects of SR59230A in primary T-ALL blasts isolated from the bone marrow of a pediatric patient at diagnosis. Treatment with SR59230A (15 μM) for 24 hours significantly reduced basal

279 respiration (p<0.001), maximal respiration (p<0.001), spare respiratory capacity (p<0.01),
280 and mitochondrial ATP production (p<0.0001) (**Fig 4A-D**). In contrast, SR59230A treatment
281 resulted in a significant increase in basal glycolysis (p<0.0001), with no detectable changes
282 in compensatory glycolysis, and a concomitant reduction in the proton efflux rate (PER)
283 derived from glycolysis (p<0.0001) (**Fig 4E-G**). ATP Rate Assay analysis showed that the
284 reduction in mitochondrial ATP production (**Fig 4H**) was only partially compensated by the
285 increased glycolytic ATP generation (**Fig 4I**), leading to a significant decrease in total cellular
286 ATP levels. These data demonstrate that SR59230A induces a bioenergetic deficit in primary
287 T-ALL blasts that cannot be fully compensated by glycolytic reprogramming.

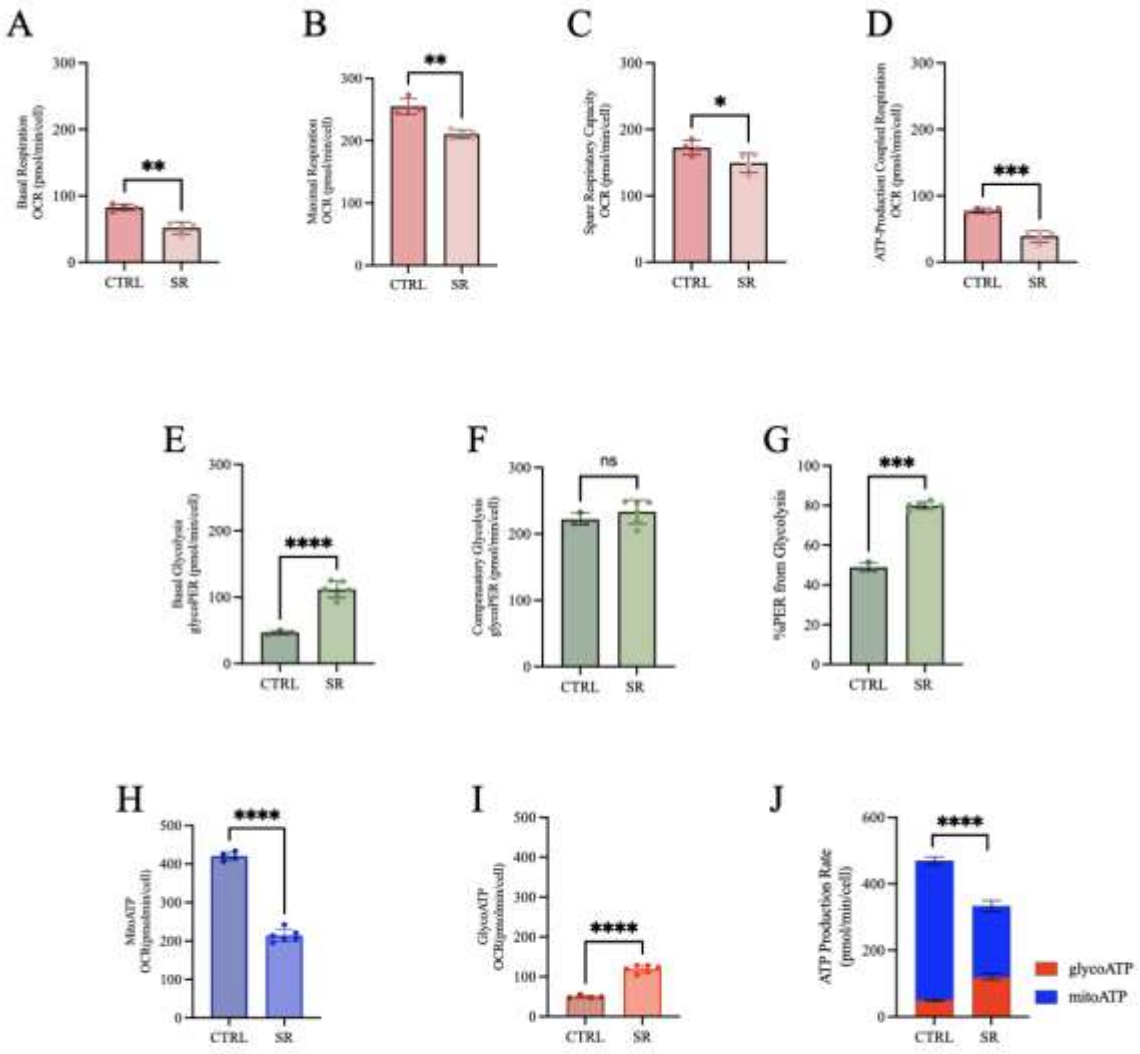

SR59230A disrupts fatty acid oxidation and exposes T-ALL to a metabolic vulnerability

Considering the marked impairment of mitochondrial respiration following SR59230A treatment, we next assessed whether this bioenergetic defect was driven by altered fatty acid oxidation (FAO).

Using the XF Long Chain Fatty Acid Oxidation Stress Test under starvation conditions to promote fatty acid uptake and HEPES (1 M) to limit extracellular acidification, we observed that SR59230A significantly reduced basal and maximal respiration, spare respiratory

capacity, and mitochondrial ATP production across all three T-ALL cell lines, both in BSA and palmitate-supplemented conditions (**Fig 5A-C**).

The comparable reduction in OCR in both settings indicates that SR59230A impairs oxidation of both endogenous and exogenous fatty acids, providing a mechanistic basis for the mitochondrial dysfunction observed in **Fig 3**.

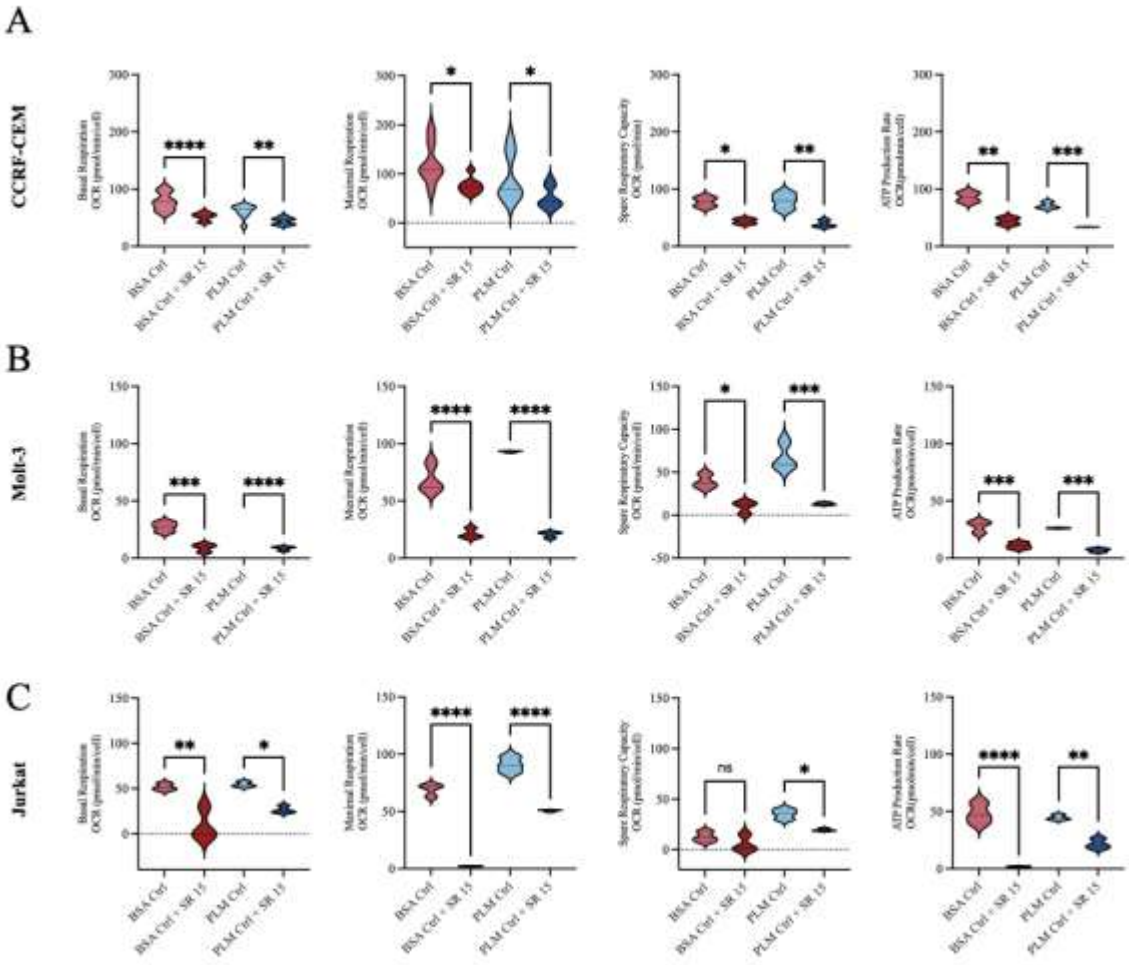

SR59230A couples fatty acid oxidation blockade to ferroptotic cell death in T-ALL

Because FAO suppression can promote the accumulation of peroxidation-prone lipids, we evaluated whether SR59230A-mediated inhibition of FAO and iron release create a

permissive environment for ferroptosis in T-ALL cells. Consistent with this model, transcript analysis revealed a significant downregulation of key ferroptosis-protective genes, including *GPX4*, *FSP1*, and *NRF2*, after 72h of SR59230A treatment in CCRF-CEM and Molt-3 cells (**Fig 6A-C**). No significant changes were observed in Jurkat cells (**Fig 6C**).

At the protein level, ferritin heavy chain (FTH1) expression remained largely unchanged in CCRF-CEM and Jurkat cells, whereas Molt-3 cells exhibited a transient increase at 24 and 48 hours of treatment (**Fig 6D** and **Fig S4D-G**). In parallel, the transferrin receptor CD71 (TFRC), a key mediator of cellular iron uptake and a determinant of intracellular iron availability, was significantly downregulated in CCRF-CEM and Molt-3 cells after 48 and 72 hours of SR59230A treatment, while it was upregulated in Jurkat cells (**Fig 6E** and **Fig S4H-L**). In support of increased cellular damage, lactate dehydrogenase A (LDHA) expression, while not specific for ferroptosis, was significantly increased in CCRF-CEM and Molt-3 cells, but remained unchanged in Jurkat cells, further underscoring the heightened sensitivity of CCRF-CEM and Molt-3 to SR59230A -induced metabolic perturbation (**Fig 6F** and **Fig S5D-F**).

Intracellular ferritin and free iron levels were quantified using the COBAS 8000 clinical diagnostic platform[35–38], routinely employed in standard patient care. Following assay optimization, treatment with the ferroptosis inducer RSL3 (0.3 μM for 3 hours) caused a significant reduction in ferritin levels across T-ALL models, confirming the suitability of this platform for detecting ferroptosis-associated alterations in iron homeostasis (**Fig 6G**). We next assessed ferritin levels following treatment with 15 μM SR59230A or the iron chelator deferoxamine (DFX; 0.1 μM) for 24h. Both treatments resulted in a significant reduction in ferritin levels in CCRF-CEM and Molt-3 cells, whereas Jurkat cells remained unaffected, consistent with their lower ferroptotic susceptibility and reduced basal FTH1 expression (**Fig 6H**).

Given the sensitivity of CCRF-CEM cells, we next performed a time-course analysis of FTH1 and iron homeostasis following SR59230A treatment to directly assess whether SR59230A progressively perturbs intracellular iron handling. We observed a progressive, time-dependent decrease in ferritin levels (**Fig 6I**), accompanied by a concomitant increase in intracellular free iron (**Fig 6J**).

To further define the engagement of ferroptotic signaling, *GPX4* expression was evaluated in all three T-ALL models treated with SR59230A (15 μM) for 24, 48, and 72 hours. A significant reduction of GPX4 protein levels was observed in CCRF-CEM cells at 24 hours (p<0.01), which became more pronounced at 72 hours (p<0.0001), whereas the other models showed no consistent modulation (**Fig 6K** and **Fig S3F-H**), underscoring the selective ferroptotic vulnerability of CCRF-CEM cells.

Finally, to functionally validate ferroptosis involvement, we evaluated whether iron chelation could mitigate SR59230A-induced cytotoxicity. Although DFX did not completely rescue cell viability under standard culture conditions (**Fig 6L**), it partially reversed SR59230A-mediated loss of viability under nutrient-starved conditions after 24 hours of treatment (**Fig 6M**).[39] Interestingly, the analysis of deregulated genes in the ferroptosis pathway within T-ALL cell line revealed markedly elevated expression of genes promoting iron metabolism-dependent ferroptosis, such as *TF, TFRC, STEAP3,* and *FTL* in CCRF-CEM and Molt-3 (**Fig 6N**), as observed in AML primary blasts.[40]

Taken together, these data indicate that SR59230A induces a ferroptosis-prone state through coordinated disruption of FAO, iron homeostasis, and GPX4-dependent antioxidant defenses.

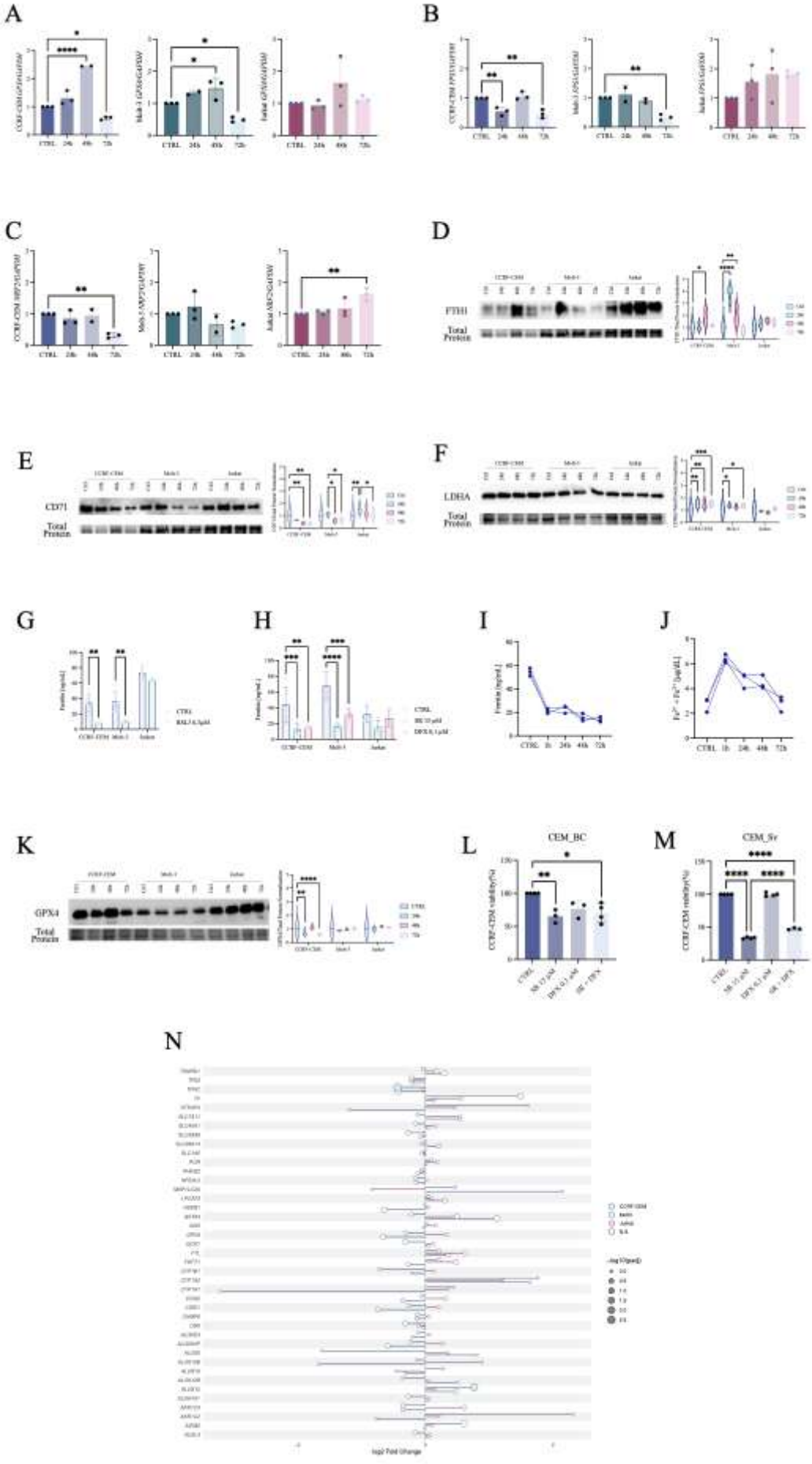
A
B
C
D
E
F
G
H
I
J
K
L
M
N
CEM_BC
CEM_Sr
CTRL
24h
48h
72h
GPX4
CD71
LDHA
FTH1
Total Protein

Discussion

Despite recent improvements in survival rates, approximately 25% of children with T-ALL experience relapse. Relapsed T-ALL is typically associated with a more aggressive clinical course and poor prognosis, highlighting a clinical need for reliable molecular markers and novel therapeutic targets capable of selectively exploiting vulnerabilities in leukemic cells.

Our work investigates the β3-AR as a previously underexplored regulator of metabolic plasticity in pediatric T-ALL. β3-AR is robustly expressed in pediatric T-ALL models, and its selective pharmacologic inhibition with SR59230A reveals metabolic liability. SR59230A induces OXPHOS transcriptional reprogramming leading to a functional collapse of mitochondrial bioenergetics, with reduced mitochondrial ATP production and FAO. SR59230A significantly affects mitochondrial respiration in CCRF-CEM and Molt-3 cells while sparing healthy counterparts. In leukemic models, substrate-specific analyses reveal that SR59230A markedly diminishes FAO, generating energetic stress that translates into heightened metabolic vulnerability. Conversely, Jurkat cells display metabolic flexibility, compensating for mitochondrial impairment by shifting toward alternative energy substrates such as glucose and glutamine, a well-recognized mechanism of treatment resistance. Real-time bioenergetic profiling and RNA-sequencing identify respiratory complex I as the main mitochondrial target of SR59230A. Complex I transcripts are consistently deregulated across all T-ALL models, underscoring coordinated mitochondrial disruption. This is highly relevant given increasing evidence that complex I inhibition (e.g., IACS-010759, EVT-701, mubritinib, or phenformin) reduces OXPHOS, rewires mitochondrial metabolism, and enhances chemosensitivity in AML, including increased cytarabine sensitivity and reduced PD-L1 and CD39 expression.[41–43] In defined genetic contexts, complex I inhibition reveals specific vulnerabilities: increased susceptibility in IDH1-mutant AML and reversal of oncogene-driven metabolic reprogramming in NOTCH1-mutant T-ALL.[44,45] Consistently,

complex I inhibitors such as metformin and intervenolin suppress tumor growth in solid tumor xenografts through tumor acidification and S6K1 dephosphorylation, independently of ATP depletion.[46,47] Our previous work in AML demonstrated that OXPHOS-high cells preferentially survive chemotherapy, and that buformin, a potent metformin analog targeting complex I, suppresses this high-OXPHOS compartment.[48] The MCL1/HK2 axis further illustrates how leukemia cells coordinate mitochondrial and glycolytic programs to endure metabolic stress.[49]

Within this framework, SR59230A disrupts mitochondrial homeostasis in T-ALL models, primarily targeting complex I and impairing OXPHOS. Metabolic analyses confirmed reduced basal respiration and spare respiratory capacity. FAO-dependent CCRF-CEM cells were particularly sensitive, whereas metabolically flexible Jurkat cells showed relative resistance, indicating that baseline fuel dependency shapes response to SR59230A. This metabolic collapse is accompanied by altered iron homeostasis, including progressive ferritin reduction and accumulation of labile iron detected by the clinically validated COBAS 8000 platform, together with downregulation of key ferroptosis defenses (*GPX4*, *FSP1* and *NRF2*). Collectively, these changes create a redox and lipid metabolic landscape permissive to ferroptosis, driving SR59230A-induced leukemic cell death.

Clinically, dysregulated iron metabolism and expanded labile iron pools promote oxidative stress in acute leukemias. In ALL, reliance on antioxidant systems such as glutathione and FSP1 creates ferroptotic vulnerability that can be therapeutically exploited by iron modulation (e.g., deferoxamine, deferasirox) or inhibition of SLC7A11 and GPX4.[50–54] Similar approaches in AML and solid tumors further support iron-dependent lipid peroxidation as a therapeutically actionable axis.[55–57] In our model, SR59230A disrupts FAO, mitochondrial respiration, and iron homeostasis, promoting lipid peroxidation and ferroptotic cell death as therapeutically exploitable vulnerability.

Modulation of the transferrin receptor (CD71) further underscores the complexity of iron handling under metabolic stress. Although reduced CD71, SR59230A-sensitive cells show FTH1 depletion and labile iron accumulation, linking diminished iron import to ferroptotic vulnerability via mitochondrial dysfunction and lipid peroxidation.[58–61] Partial rescue by iron chelation supports this mechanism and highlights ferritin-dependent iron buffering as a therapeutically actionable axis. Consistently, reduced FTH1 expression sensitizes leukemic stem cells to iron-targeting interventions and mitochondrial injury, thereby identifying ferritin-dependent iron buffering as a therapeutically exploitable axis.[62–65]

Importantly, integration of clinically validated iron parameters into our framework establishes a direct translational bridge, enabling extension of these mechanistic insights to patient-derived samples explored in a clinical context.

Clinically, the use of an automated COBAS 8000 platform anchors these mechanistic findings in diagnostically accessible metrics.

However, our findings are largely based on established T-ALL cell line models, which may not fully capture disease heterogeneity and microenvironmental context, and the number of patient-derived samples is limited. In addition, while SR59230A was used to interrogate β3-AR function, potential off-target effects cannot be excluded. These aspects will be the focus of future studies.

In conclusion, SR59230A induces a metabolic crisis in pediatric T-ALL characterized by complex I–driven OXPHOS disruption, impaired FAO, iron homeostasis perturbation, and suppression of ferroptosis defense. The convergence of mitochondrial dysfunction, lipid metabolic stress, and iron dysregulation sensitizes leukemic cells to ferroptotic death, positioning B3AR blockade as a potential metabolic-oriented therapeutic strategy in pediatric T-ALL.

Abbreviation

ALL	acute lymphoblastic leukemia
AML	acute myeloid leukemia
BM	bone marrow
DEGs	differentially expressed genes
DFX	deferoxamine
ECLIA	electrochemiluminescence immunoassay
FAO	fatty acid oxidation
FTH1	ferritin heavy chain
GPX4	glutathione peroxidase 4
LDHA	lactate dehydrogenase A
NRF2	nuclear factor erythroid derived 2
OXPHOS	oxidative phosphorylation
PER	proton efflux rate
STEAP3	ferrireductas
T-ALL	T-cell acute lymphoblastic leukemia
TF	transferrin
TFRC	transferrin receptor CD71
β3-AR	β3-adrenergic receptor

Declaration of Competing Interest

The authors declare no competing interests.

Author Contributions

CB, ST, and MC conceived the study and designed the research; CB, RA, FC, MA, GM, FDL, LB, AR, and FP established and optimized the experimental methodology; CB, RA,

FC, and MA performed experiments and acquired data; CB and ST prepared the figures and visualizations; AT, MV, and MC supervised the project and provided conceptual guidance; CB and ST wrote the original draft; and CB, ST, AR, FP,EC, AT, MV, and MC reviewed and edited the manuscript. All authors read and approved the final version.

Conflict-of-interest disclosure

The authors declare no competing financial interests.

Acknowledgments

This work was supported by SIES-Beat Leukemia through the Postdoctoral Fellowship 2024 awarded to Cristina Banella and by the “Il sorriso di Martina” Foundation. We are grateful to Claudio Favre for helpful discussions and support throughout the course of this study.

Figure Legends

Figure 1: Selective targeting of ADRB3 impairs T-ALL cell viability while sparing normal PBMCs.

(A) Flow cytometry analysis showing elevated β3-adrenergic receptor (ADRB3) expression in T-ALL cell line models compared with normal peripheral blood mononuclear cells (PBMCs) (A). Viability of PBMCs and T-ALL cell lines treated with the selective ADRB3 antagonist SR59230A (0–50 μM). PBMC viability remained unaffected, whereas T-ALL cells displayed a dose- and time-dependent reduction under basal (B) and serum-starved conditions (C). Selectivity of SR59230A treatment on β-adrenergic receptor isoforms. No significant changes were observed in expression level of *ADRB1* (D) or *ADRB2* (E) following treatment, whereas *ADRB3* expression was significantly modulated (F). Densiometric scanning of ADRB3 expression levels after normalization with total protein content per lane in T-ALL cell line models (G). Blot shown represent the best exposure times selected from multiple experiments, with dividing lines indicating where images have been cropped from different parts of the same gel or from different gels. Full-length blots with multiple exposure times are provided in the Fig S1. The results correspond to three independent experiments. Data are presented as mean ± SD. Statistical significance was assessed by Two-way Anova, multiple comparisons followed by Tukey post-hoc test (* p=0.001; *** p=0.0001; **** p≤0.0001).

Figure 2: RNAseq analysis following β3-AR inhibition in T-ALL cell lines.

(A) Hallmark pathway enrichment analysis (GSEA) across the three T-ALL cell lines. Box plots display normalized enrichment scores (NES) of significantly modulated pathways. (B) Schematic representation of the mitochondrial respiratory chain highlighting leading edge genes contributing to OXPHOS pathway enrichment. (C) Venn diagram illustrating the

overlap of DEGs across the three cell lines upon β3-AR inhibition (filtering criteria: p-value <0.05; FDR <0.1).

Figure 3: SR59230A impairs mitochondrial respiration and glycolysis efficiency in T-ALL cells model.

Mitochondrial respiration was assessed in CCRF-CEM, Molt-3, and Jurkat cells following 24-h treatment with SR59230A 15 μM using the Cell Mito Stress Test. Basal respiration (A), maximal respiration (B), spare respiratory capacity (C), and ATP-linked respiration (D) are shown. Substrate dependency was evaluated using the Substrate Oxidation Stress Test. Coupling efficiency following inhibition of glutamine oxidation (BPTES), pyruvate transport (UK5099), or fatty acid oxidation (PRX) was determined to define mitochondrial reliance on specific fuel sources at baseline and after 24 h SR59230A treatment in CCRF-CEM (E), Molt-3 (F), and Jurkat (G) cells. Glycolytic parameters were assessed by Glycolytic Rate Assay, including basal glycolysis (H) and compensatory glycolysis (I) following SR59230A treatment. Data represent three independent experiments performed in triplicate and are shown as mean ± SD. Statistical significance was determined using the two-tailed Student's *t* test. *p<0.05; **p<0.005; ***p<0.0005; ****p<0.0001.

Figure 4: SR59230A disrupts mitochondrial bioenergetics in primary pediatric T-ALL blasts.

Primary T-ALL blasts isolated from the bone marrow of a pediatric patient at diagnosis were treated with SR 15 μM for 24 h. Mitochondrial respiration was assessed using the Cell Mito Stress Test, evaluating basal respiration (A), maximal respiration (B), spare respiratory capacity (C), and ATP-linked respiration (D). Glycolytic function was analyzed by Glycolytic Rate Assay, showing increased basal glycolysis (E), and a significant increase in the percentage of proton efflux rate derived from glycolysis (%PER from glycolysis) (G) following

SR59230A treatment. Total cellular ATP production was determined by ATP Rate Assay. SR59230A treatment resulted in a reduction in mitochondrial ATP production (H), accompanied by an increase in glycolytic ATP production (I); however, total ATP production was overall decreased after treatment. Data are presented as mean ± SD of technical replicates. Statistical analysis was performed using the two-tailed Student's *t* test. *P < .05; **p<0.005; ***p<0.0005; ****p<0.0001.

Figure 5: SR59230A impairs endogenous and exogenous fatty acid–driven mitochondrial respiration in T-ALL cells.

Long-chain fatty acid oxidation was assessed using the Palmitate Oxidation Stress Test. Mitochondrial respiration parameters—including basal respiration, maximal respiration, spare respiratory capacity, and ATP production rate—were measured under basal conditions and after 24-hour treatment with SR59230A (15 μM) in both BSA control conditions (reflecting endogenous fatty acid oxidation) and palmitate-BSA–supplemented conditions (reflecting exogenous fatty acid oxidation). Results are shown for CCRF-CEM (A), Molt-3 (B), and Jurkat (C) cells. Data represent three independent experiments performed in triplicate and are shown as mean ± SD. Statistical significance was determined using the two-tailed Student's *t* test. *p<0.05; **p<0.005; ***p<0.0005; ****p<0.0001.

Figure 6: SR59230A induces ferroptosis-associated transcriptional and iron metabolic remodeling in T-ALL cells.

Transcript levels of ferroptosis-protective genes, including *GPX4* (A), *FSP1* (B), and *NRF2* (C), were evaluated after 24, 48, and 72 h of SR59230A 15 μM treatment. Protein expression of iron metabolism–related markers FTH1 (D) and CD71 (E), as well as the cellular stress marker LDHA (F), was assessed by Western blot at the indicated time points. Ferritin levels were quantified using the COBAS 8000 clinical diagnostic platform following treatment with

the ferroptosis inducer RSL3 (3 μM, 3 hours) (G), or after 24-h with SR59230A 15 μM or deferoxamine (DFX; 0.1 μM) (H). A time-course analysis (1–72 hours) of ferritin levels following SR59230A treatment was performed using COBAS 8000 (I), with concomitant measurement of intracellular free iron levels in CCRF-CEM (J). GPX4 protein expression was analyzed by Western blot in all T-ALL cell lines following 24, 48, and 72 hours of SR59230A (15 μM) treatment (K). Cell viability of CCRF-CEM cells was assessed after treatment with SR59230A, DFX, or their combination under standard culture conditions (L) or nutrient-starved conditions (M). Data are representative of at least three independent experiments. Statistical analyses were performed using the two-tailed Student's *t* test or nonparametric tests where appropriate. *p<0.05; **p<0.005; ***p<0.0005; ****p<0.0001. (N) Lollipop plot displaying significantly upregulated genes regulating ferroptosis in AML cells. Gene expression levels were normalized using Z-score transformation.

Supplemental Information

All data needed to evaluate the conclusions in the paper are present in the main text and/or the Supplementary Materials.

Ethical statement

The study was approved by the Comitato Etico Regionale della Toscana – Pediatrico (protocol number CET_14/2023). All procedures were conducted in accordance with the Declaration of Helsinki and applicable institutional and national ethical guidelines.

References

1. Karrman, K. & Johansson, B. Pediatric T-cell acute lymphoblastic leukemia. *Genes Chromosomes Cancer* **56**, 89–116 (2017).
2. Hofmans, M. *et al.* Results of successive EORTC-CLG 58 881 and 58 951 trials in paediatric T-cell acute lymphoblastic leukaemia (ALL). *Br. J. Haematol.* **186**, 741–753 (2019).
3. Winter, S. S. *et al.* Improved Survival for Children and Young Adults With T-Lineage Acute Lymphoblastic Leukemia: Results From the Children's Oncology Group AALL0434 Methotrexate Randomization. *Journal of Clinical Oncology* **36**, 2926–2934 (2018).
4. Burns, M. A. *et al.* Identification of prognostic factors in childhood T-cell acute lymphoblastic leukemia: Results from DFCI ALL Consortium Protocols 05-001 and 11-001. *Pediatr. Blood Cancer* **68**, (2021).
5. Pui, C.-H., Robison, L. L. & Look, A. T. Acute lymphoblastic leukaemia. *The Lancet* **371**, 1030–1043 (2008).
6. Stanulla, M. & Schrappe, M. Treatment of Childhood Acute Lymphoblastic Leukemia. *Semin. Hematol.* **46**, 52–63 (2009).
7. Bassan, R. & Hoelzer, D. Modern Therapy of Acute Lymphoblastic Leukemia. *Journal of Clinical Oncology* **29**, 532–543 (2011).
8. Hurtz, C. *et al.* Oncogene-independent BCR-like signaling adaptation confers drug resistance in Ph-like ALL. *Journal of Clinical Investigation* **130**, 3637–3653 (2020).
9. Lin, Z. *et al.* Metabolic reprogramming promotes apoptosis resistance in acute lymphoblastic leukemia through CASP3 lactylation. *Mol. Cancer* **24**, 204 (2025).
10. Huang, F.-L., Yu, S.-J. & Li, C.-L. Role of Autophagy and Apoptosis in Acute Lymphoblastic Leukemia. *Cancer Control* **28**, (2021).
11. Mezzatesta, C. & Bornhauser, B. C. Exploiting Necroptosis for Therapy of Acute Lymphoblastic Leukemia. *Front. Cell Dev. Biol.* **7**, (2019).
12. Mesbahi, Y., Trahair, T. N., Lock, R. B. & Connerty, P. Exploring the Metabolic Landscape of AML: From Haematopoietic Stem Cells to Myeloblasts and Leukaemic Stem Cells. *Front. Oncol.* **12**, (2022).
13. Noguera, N. I., Hasan, S. K., Ammatuna, E. & Venditti, A. Editorial: Metabolic Rewiring in Leukemias. *Front. Oncol.* **11**, (2021).
14. Hao, X. *et al.* Metabolic reprogramming and immune regulation in acute myeloid leukemia. *Front. Immunol.* **16**, (2025).
15. Shi, X., Feng, M. & Nakada, D. Metabolic dependencies of acute myeloid leukemia stem cells. *Int. J. Hematol.* **120**, 427–438 (2024).
16. Issa, G. C. & DiNardo, C. D. Acute myeloid leukemia with IDH1 and IDH2 mutations: 2021 treatment algorithm. *Blood Cancer J.* **11**, 107 (2021).
17. Cerchione, C. *et al.* IDH1/IDH2 Inhibition in Acute Myeloid Leukemia. *Front. Oncol.* **11**, (2021).
18. Fruchtman, H., Avigan, Z. M., Waksal, J. A., Brennan, N. & Mascarenhas, J. O. Management of isocitrate dehydrogenase 1/2 mutated acute myeloid leukemia. *Leukemia* **38**, 927–935 (2024).
19. Pollyea, D. A., Amaya, M., Strati, P. & Konopleva, M. Y. Venetoclax for AML: changing the treatment paradigm. *Blood Adv.* **3**, 4326–4335 (2019).
20. Pollyea, D. A. *et al.* Venetoclax with azacitidine disrupts energy metabolism and targets leukemia stem cells in patients with acute myeloid leukemia. *Nat. Med.* **24**, 1859–1866 (2018).
21. Niscola, P. *et al.* Venetoclax and new BCL-2 inhibitors in acute myeloid leukemia. *Expert Opin. Pharmacother.* **26**, 1725–1739 (2025).

22. Ramsey, H. E. *et al.* A Novel MCL1 Inhibitor Combined with Venetoclax Rescues Venetoclax-Resistant Acute Myelogenous Leukemia. *Cancer Discov.* **8**, 1566–1581 (2018).
23. Rahmani, M. *et al.* Cotargeting BCL-2 and PI3K Induces BAX-Dependent Mitochondrial Apoptosis in AML Cells. *Cancer Res.* **78**, 3075–3086 (2018).
24. Chen, X. *et al.* Targeting Mitochondrial Structure Sensitizes Acute Myeloid Leukemia to Venetoclax Treatment. *Cancer Discov.* **9**, 890–909 (2019).
25. Pullarkat, V. A. *et al.* Venetoclax and Navitoclax in Combination with Chemotherapy in Patients with Relapsed or Refractory Acute Lymphoblastic Leukemia and Lymphoblastic Lymphoma. *Cancer Discov.* **11**, 1440–1453 (2021).
26. Lato, M. W., Przysucha, A., Grosman, S., Zawitkowska, J. & Lejman, M. The New Therapeutic Strategies in Pediatric T-Cell Acute Lymphoblastic Leukemia. *Int. J. Mol. Sci.* **22**, 4502 (2021).
27. Cao, H.-Y. *et al.* Venetoclax plus azacitidine in relapsed or refractory T-cell acute lymphoblastic leukaemia: a multicentre, single-arm, phase 2 trial. *Lancet Haematol.* **12**, e946–e955 (2025).
28. da Silva-Diz, V. & Herranz, D. Unleashing the Full Potential of Metabolic Interventions in T-ALL. *Blood Cancer Discov.* **6**, 163–167 (2025).
29. Dal Monte, M. *et al.* β-Adrenoceptors as drug targets in melanoma: novel preclinical evidence for a role of β_3 -adrenoceptors. *Br. J. Pharmacol.* **176**, 2496–2508 (2019).
30. Calvani, M. *et al.* β3-Adrenoreceptor Blockade Reduces Hypoxic Myeloid Leukemic Cells Survival and Chemoresistance. *Int. J. Mol. Sci.* **21**, 4210 (2020).
31. Preitner, F. *et al.* Metabolic response to various *β* -adrenoceptor agonists in β_3 -adrenoceptor knockout mice: Evidence for a new *β* -adrenergic receptor in brown adipose tissue. *Br. J. Pharmacol.* **124**, 1684–1688 (1998).
32. Calmasini, F. B. *et al.* Long-term treatment with the beta-3 adrenoceptor agonist, mirabegron ameliorates detrusor overactivity and restores cyclic adenosine monophosphate (cAMP) levels in obese mice. *Neurourol. Urodyn.* **36**, 1511–1518 (2017).
33. Gao, X., Li, Y. & Jiang, Z. β$_3$-Adrenoceptor activation upregulates apolipoprotein A-I expression in HepG2 cells, which might further promote cholesterol efflux from macrophage foam cells. *Drug Des. Devel. Ther.* **Volume11**, 617–627 (2017).
34. Dal Monte, M. *et al.* Functional involvement of β3-adrenergic receptors in melanoma growth and vascularization. *J. Mol. Med.* **91**, 1407–1419 (2013).
35. Bohn, M. K. *et al.* Paediatric reference intervals for 17 Roche cobas 8000 e602 immunoassays in the CALIPER cohort of healthy children and adolescents. *Clinical Chemistry and Laboratory Medicine (CCLM)* **57**, 1968–1979 (2019).
36. Wan, B. *et al.* Analytical performance and workflow evaluation of the Roche E170 modular immunoassay analyzer in a pediatric setting. *Clin. Biochem.* **38**, 262–271 (2005).
37. Hou, L. *et al.* Analytical evaluation of three soluble transferrin receptor measurement systems for diagnosis of iron deficiency anemia: A retrospective study. *J. Clin. Lab. Anal.* **34**, (2020).
38. Kolbe-Busch, S. *et al.* Multicenter Evaluation of a Fully Mechanized Soluble Transferrin Receptor Assay on the Hitachi and Cobas Integra Analyzers. The Determination of Reference Ranges. *Clin. Chem. Lab. Med.* **40**, (2002).
39. Wang, B., Wang, H.-L., Ye, Y.-F., Song, J.-Z. & Li, J. Ferroptosis regulation and acute leukemia: Mechanisms and therapeutic perspectives. *Biochem. Biophys. Res. Commun.* **800**, 153284 (2026).
40. Wang, B., Wang, H.-L., Ye, Y.-F., Song, J.-Z. & Li, J. Ferroptosis regulation and acute leukemia: Mechanisms and therapeutic perspectives. *Biochem. Biophys. Res. Commun.* **800**, 153284 (2026).

41. Baccelli, I. *et al.* Mubritinib Targets the Electron Transport Chain Complex I and Reveals the Landscape of OXPHOS Dependency in Acute Myeloid Leukemia. *Cancer Cell* **36**, 84-99.e8 (2019).
42. Luna-Yolba, R. *et al.* Disrupting Mitochondrial Electron Transfer Chain Complex I Decreases Immune Checkpoints in Murine and Human Acute Myeloid Leukemic Cells. *Cancers (Basel).* **13**, 3499 (2021).
43. Bassal, M. A. *et al.* Author Correction: Germline mutations in mitochondrial complex I reveal genetic and targetable vulnerability in IDH1-mutant acute myeloid leukaemia. *Nat. Commun.* **13**, 4131 (2022).
44. Baran, N. *et al.* Inhibition of mitochondrial complex I reverses NOTCH1-driven metabolic reprogramming in T-cell acute lymphoblastic leukemia. *Nat. Commun.* **13**, 2801 (2022).
45. Guo, S. *et al.* Mitochondrial dysfunction fuels drug resistance in adult T-cell acute lymphoblastic leukemia. *J. Transl. Med.* **23**, 542 (2025).
46. Yap, T. A. *et al.* Complex I inhibitor of oxidative phosphorylation in advanced solid tumors and acute myeloid leukemia: phase I trials. *Nat. Med.* **29**, 115–126 (2023).
47. Yoshida, J. *et al.* Mitochondrial complex I inhibitors suppress tumor growth through concomitant acidification of the intra- and extracellular environment. *iScience* **24**, 103497 (2021).
48. Banella, C. *et al.* Ascorbate Plus Buformin in AML: A Metabolic Targeted Treatment. *Cancers (Basel).* **14**, 2565 (2022).
49. Catalano, G. *et al.* MCL1 regulates AML cells metabolism via direct interaction with HK2. Metabolic signature at onset predicts overall survival in AMLs' patients. *Leukemia* **37**, 1600–1610 (2023).
50. Pontel, L. B. *et al.* Acute lymphoblastic leukemia necessitates GSH-dependent ferroptosis defenses to overcome FSP1-epigenetic silencing. *Redox Biol.* **55**, 102408 (2022).
51. Han, J., Yang, Y., Wei, Y., Jin, J. & Feng, W. Ferroptosis: a new dawn in the treatment of acute lymphoblastic leukemia. *Front. Oncol.* **15**, (2026).
52. Wang, B., Wang, H.-L., Ye, Y.-F., Song, J.-Z. & Li, J. Ferroptosis regulation and acute leukemia: Mechanisms and therapeutic perspectives. *Biochem. Biophys. Res. Commun.* **800**, 153284 (2026).
53. Lyu, T., Li, X. & Song, Y. Ferroptosis in acute leukemia. *Chin. Med. J. (Engl).* **136**, 886–898 (2023).
54. Tavakoli, F. *et al.* Ferroptosis in AML: nanoparticles, biomarkers, and immune rewiring for therapeutic breakthroughs. *Discover Oncology* **16**, 1937 (2025).
55. Ubellacker, J. M. *et al.* Lymph protects metastasizing melanoma cells from ferroptosis. *Nature* **585**, 113–118 (2020).
56. Perera, L., Brown, S. M., Silver, B. B., Tokar, E. J. & Sinha, B. K. Ferroptosis Inducers Erastin and RSL3 Enhance Adriamycin and Topotecan Sensitivity in ABCB1/ABCG2-Expressing Tumor Cells. *Int. J. Mol. Sci.* **26**, 635 (2025).
57. Li, D. *et al.* Silencing TRPM2 enhanced erastin- and RSL3-induced ferroptosis in gastric cancer cells through destabilizing HIF-1α and Nrf2 proteins. *Cytotechnology* **74**, 559–577 (2022).
58. Kollia, P. *et al.* Molecular evidence for transferrin receptor 2 expression in all FAB subtypes of acute myeloid leukemia. *Leuk. Res.* **27**, 1101–1103 (2003).
59. Kollia, P. *et al.* Molecular evidence for transferrin receptor 2 expression in all FAB subtypes of acute myeloid leukemia. *Leuk. Res.* **27**, 1101–1103 (2003).

60. Ivanova, T. I. *et al.* Prognostic Value of Serum Transferrin Analysis in Patients with Ovarian Cancer and Cancer-Related Functional Iron Deficiency: A Retrospective Case–Control Study. *J. Clin. Med.* **11**, 7377 (2022).
61. Liu, Q. *et al.* Significance of CD71 expression by flow cytometry in diagnosis of acute leukemia. *Leuk. Lymphoma* **55**, 892–898 (2014).
62. Wei, J. *et al.* Dipetidyl peptidase-4 and transferrin receptor serve as prognostic biomarkers for acute myeloid leukemia. *Ann. Transl. Med.* **9**, 1381–1381 (2021).
63. Bertoli, S. *et al.* Ferritin heavy/light chain (FTH1/FTL) expression, serum ferritin levels, and their functional as well as prognostic roles in acute myeloid leukemia. *Eur. J. Haematol.* **102**, 131–142 (2019).
64. Reikvam, H. *et al.* Ferritin in Acute Myeloid Leukemia: Not Only a Marker of Inflammation and Iron Overload, but Also a Regulator of Cellular Iron Metabolism, Signaling and Communication. *Int. J. Mol. Sci.* **26**, 5744 (2025).
65. Parry, D. H., Worwood, M. & Jacobs, A. Serum Ferritin in Acute Leukaemia at Presentation and during Remission. *BMJ* **1**, 245–247 (1975).

Supplementary Files

This is a list of supplementary files associated with this preprint. Click to download.

- SupplementalFigureMaterials.docx